Fluorinated interphase enables reversible Zn^{2+} storage in aqueous $ZnSO_4$ electrolytes

Yuhang Dai,[1,3,‡] Jiantao Li,[2,‡,*] Chengyi Zhang,[5,‡] Ruihu Lu,[5] Xiafang Tao,[4] Kwadwo Asare Owusu,[6] Guanjie He,[3] Yazhou Zhou,[4,*] Jun Lu[1,2,*]

[1]College of Chemical and Biological Engineering, Zhejiang University, Hangzhou 310027, People's Republic of China

[2]Chemical Sciences and Engineering Division, Argonne National Laboratory Lemont, IL 60439, USA

[3]Electrochemical Innovation Lab, Department of Chemical Engineering, University College London, London WC1E 7JE, UK

[4]Max Planck Institute for Polymer Research, Mainz 55128, Germany

[5]School of Chemical Sciences, The University of Auckland, Auckland 1010, New Zealand

[6]Department of Chemical Sciences and Bernal Institute, University of Limerick, Limerick V94 T9PX, Ireland

ABSTRACT

Aqueous zinc-ion batteries (AZIBs) using $ZnSO_4$ aqueous electrolytes complement Li-ion batteries and offer high safety, low cost, and scalability. However, an inferior cycle life, attributed to the generation of basic layered double hydroxides (LDHs) on the cathode during cycling, hampers the development of AZIBs. Although $Zn(CF_3SO_3)_2$ ($Zn(OTf)_2$) electrolytes demonstrate

exceptional performance, their higher cost in comparison to $ZnSO_4$ offsets their electrochemical stability benefits. Toward this end, we propose a fluorinated interphase strategy to achieve a stable battery with $ZnSO_4$ electrolytes by in situ pre-constructing the cathode-electrolyte interphase (CEI) of ZnOTf-LDH on the cathode surface. Unlike $ZnSO_4$-LDH, which obstructs the diffusion channel of zinc ions, ZnOTf-LDH facilitates the desolvation of zinc ions, thereby enhancing the cycling stability (over 50 cycles at a low current density of 200 mA g^{-1}). This work offers valuable insights into the degradation mechanism of AZIBs and provides an effective approach for developing stable and low-cost AZIBs.

TOC GRAPHICS

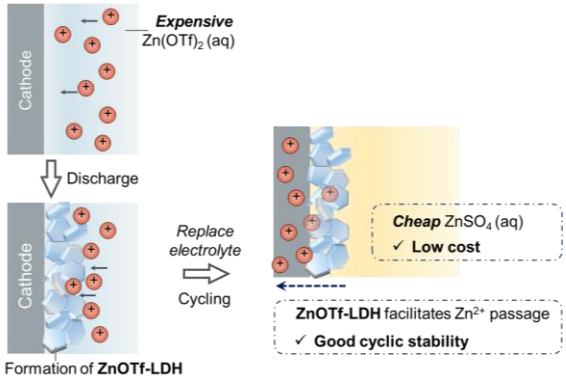

Current electrochemical energy storage devices predominantly rely on lithium-ion batteries (LIBs). However, LIBs exhibit inherent limitations concerning safety, availability, sustainability, and cost[1]. Similar to LIBs, rechargeable aqueous zinc-ion batteries (AZIBs) also employ Zn^{2+} to shuttle between electrodes[2]. Typically, AZIBs incorporate vanadium-based or manganese-based materials as cathodes, $ZnSO_4$ or $Zn(CF_3SO_3)_2$, ($Zn(OTf)_2$) as the electrolyte, and zinc foil as the anode[3]. Due to the use of zinc metal anode, AZIBs possess low redox potential (-0.76 V versus

standard hydrogen electrode), high theoretical capacity (820 mAh g^{-1}), non-flammability, and low cost, rendering them promising candidates for large-scale energy storage applications[4-11]. However, the practical implementation of AZIBs has faced significant hurdles[12,13], especially due to the fact that although the cost-effective $ZnSO_4$ (~0.04 USD g^{-1}) has been deemed the most promising candidate for commercializing AZIBs, its inadequate cation-anion separation leads to a limited battery cycle life[14]. Conversely, the $Zn(OTf)_2$ electrolyte, which contains large anion groups, demonstrates a satisfactory cycle life but is over ten times more expensive (~8.7 USD g^{-1}) than $ZnSO_4$ and poses environmental concerns[15,16].

It has been noted that the use of aqueous solvents in both $ZnSO_4$ and $Zn(OTf)_2$ electrolytes can cause undesired side reactions at the cathode-electrolyte interface[17]. In particular, the intercalation of Zn^{2+} accompanied by the intercalation of H^+ results in excess OH^- in the local environment, which may potentially affect the battery performance. This then enables the formation of Zn-based layered double hydroxides (LDHs), such as $Zn_4SO_4(OH)_6{\cdot}nH_2O$ and $Zn_x(OTf)_y(OH)_{2x-y}{\cdot}nH_2O$ in corresponding electrolytes[18-22]. Given that such LDHs would be present at the cathode-electrolyte interphase throughout the reaction once formed[23], their composition/structure may significantly influence the cycling stability[24]. While major efforts have been devoted to building stable host cathodes such as pre-intercalation, defect engineering, and morphological regulation[25,26], there is still a lack of investigations on the intrinsic properties of these LDHs[27,28]. For example, $Zn_x(OTf)_y(OH)_{2x-y}{\cdot}nH_2O$ and $Zn_4SO_4(OH)_6{\cdot}nH_2O$ expose -OTf[29] and $-SO_4$ surface groups[24], respectively. The water-repelling effect of -OTf groups may create a water-poor Inner Helmholtz Plane (IHP) while $-SO_4$ may not have the same effect[30]. Elucidating the nature of the above LDHs would inspire a profound understanding of the more stable cycle of AZIBs in $Zn(OTf)_2$ than in $ZnSO_4$, which has not yet been explored.

Here, we propose a fluorinated interphase strategy to achieve stable AZIBs in $ZnSO_4$ electrolytes based on an in-depth understanding of the intrinsic properties of $ZnSO_4$-LDH and ZnOTf-LDH. We demonstrate that $ZnSO_4$-LDH would block Zn^{2+} diffusion channels and result in rapid capacity fading, while ZnOTf-LDH promotes desolvation of hydrated Zn^{2+} before Zn^{2+} intercalation due to abundant $-CF_3$ groups within its channel. Through in-situ growth of a thin CEI layer of ZnOTf-LDH on the cathode surface by pre-cycling the cathode in $Zn(OTf)_2$ electrolyte, the constructed battery delivers stable cycling in $ZnSO_4$ electrolyte over 50 cycles at a low current density (200 mA g^{-1}). This thin ZnOTf-LDH does not increase the cost but contributes to better stability significantly. This concept of a channel that repels water but absorbs Zn^{2+} inspires the design of other electrode-electrolyte interphases needed to prevent side reactions involving water.

The structures of ZnOTf-LDH and $ZnSO_4$-LDH were established to theoretically investigate their effect on Zn^{2+} storage. We can observe that the ZnOTf-LDH possesses channels between an adjacent lamellar structure with a width of 5.1 Å, which is larger than that of $ZnSO_4$-LDH (3.1 Å) (Figure 1a,c). This can be attributed to the hydrophobic character of exposed $-CF_3$ groups. Benefiting from that, the crystalline water mainly occupies the middle of the channels, leaving a space for the rapid migration of Zn^{2+} during discharging process (Figure 1a).

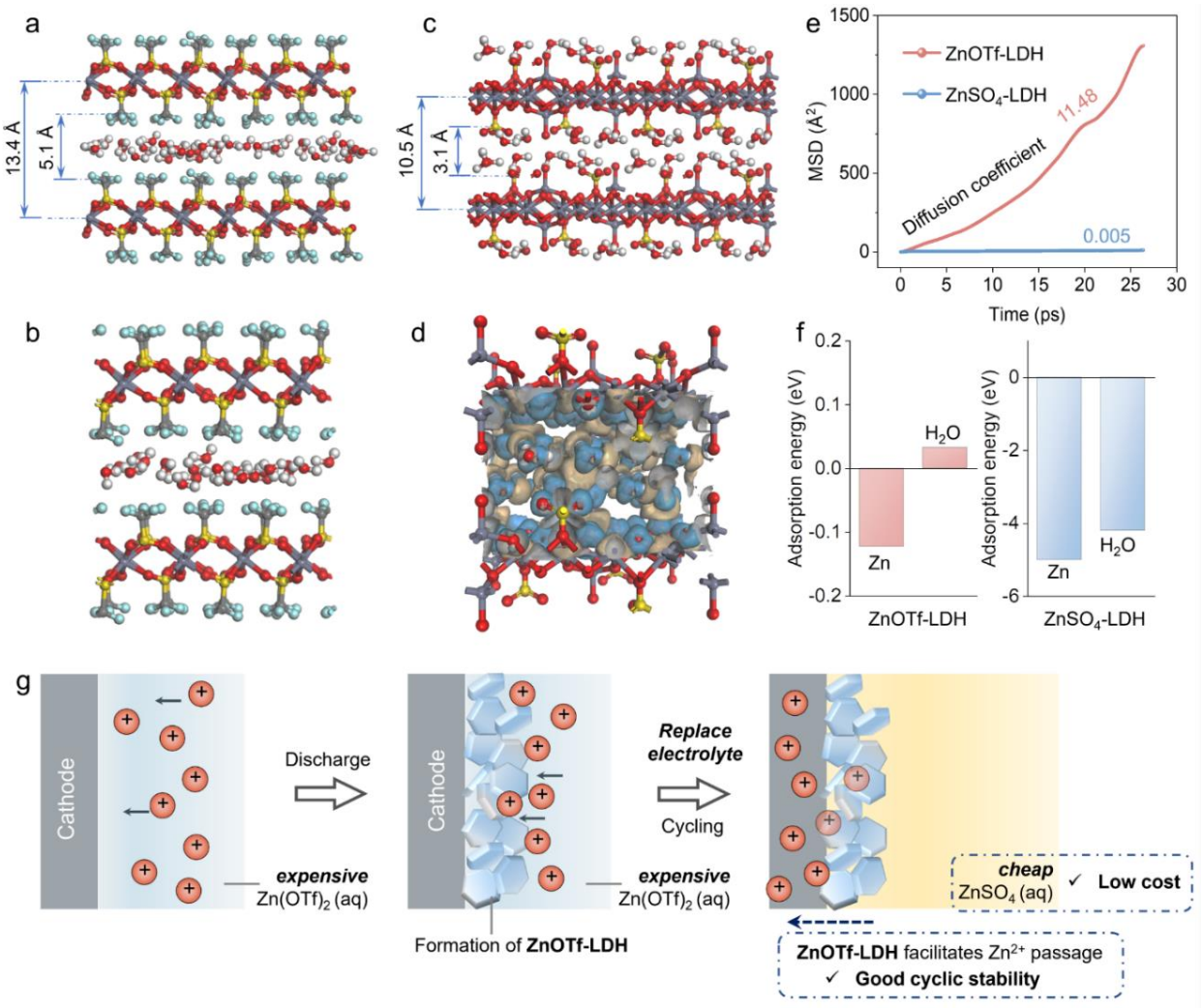

Figure 1. Theoretical calculations. (a, c) Optimized structures of ZnOTf-LDH and $ZnSO_4$-LDH. (b, d) Magnification and charge density difference plots in ZnOTf-LDH and $ZnSO_4$-LDH. (e) Diffusion coefficient of Zn^{2+} in ZnOTf-LDH and $ZnSO_4$-LDH by molecular dynamics simulations. (f) Comparison of adsorption energies of Zn and H_2O on ZnOTf-LDH and $ZnSO_4$-LDH. (g) Schematic illustration of the proposed strategy. After the formation of ZnOTf-LDH on the cathode surface in the $Zn(OTf)_2$ electrolyte, the battery can cycle stably with the $ZnSO_4$ electrolyte.

In contrast, within the $ZnSO_4$-LDH, the crystalline water binds to the $-SO_4$ groups, blocking the narrow channels for Zn^{2+} diffusion (Figure 1c). Charge density simulations were further employed to investigate the interaction between Zn^{2+} and the host LDHs. For ZnOTf-LDH, no

electron transfer occurs, which suggests no bonding between water and the -CF_3 group (Figure 1b). Thus, water with good mobility can go through these channels, leading to the free movement of Zn^{2+}. As opposed to the ZnOTf-LDH, stable hydrogen-bonding networks are formed between the water and -SO_4 group in the $ZnSO_4$-LDH, significantly hindering Zn^{2+} (Figure 1d). Indeed, the diffusion coefficient of Zn^{2+} calculated by the first-principle molecular dynamics is 11.48 in ZnOTf-LDH, which is 3 orders of magnitude higher than that of $ZnSO_4$-LDH (0.005) (Figure 1e). Remarkably, the ZnOTf-LDH structure is maintained well after 10 ps, while it collapses in the $ZnSO_4$-LDH (Figure S1a,b), indicating superior stability of ZnOTf-LDH. Moreover, Figures 1f, S1c, and S1d revealed the interactions between the LDHs and external H_2O molecules. As stated above, -CF_3 is hydrophobic, and -SO_4 is hydrophilic, enabling $ZnSO_4$-LDH to adsorb external H_2O tightly with an adsorption energy of -4.2 eV. In comparison, the ZnOTf-LDH repels external H_2O with an adsorption energy of 0.033 eV (Figure 1f). As a result, H_2O can be sufficiently removed during the intercalation of solvated Zn^{2+} due to numerous -CF_3 groups within the channel of ZnOTf-LDH. The combination of available diffusion channels and desolvation-assisted effects could help us understand the better cycling performance in $Zn(OTf)_2$ than in $ZnSO_4$ electrolytes.

According to the theoretical calculations, the ZnOTf-LDH interphase could be sufficient (without using the $Zn(OTf)_2$ electrolyte) to achieve stable cycling of AZIBs. Therefore, we propose to pre-cycle the cathode material in a small amount of expensive $Zn(OTf)_2$ electrolyte to in-situ generate the ZnOTf-LDH interphase. The cathode is then placed in a normal amount of inexpensive $ZnSO_4$ electrolyte for formal cycling tests, thus achieving stable cycling of aqueous Zn-ion batteries based on the low cost (Figure 1g).

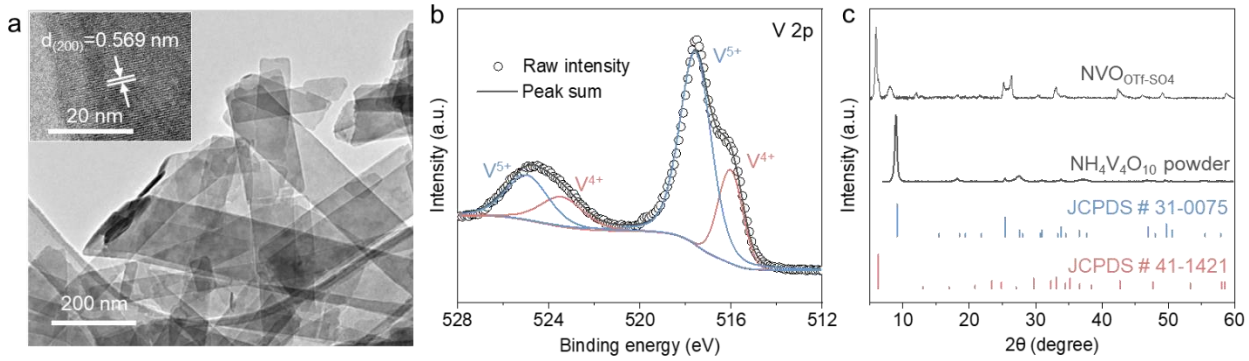

Figure 2. (a) Transmission electron microscope (TEM) and corresponding high-resolution TEM image (inset) of the pristine $NH_4V_4O_{10}$. (b) X-ray photoelectron spectroscopy spectrum of the pristine $NH_4V_4O_{10}$. (c) X-ray diffraction patterns including pristine $NH_4V_4O_{10}$ powder and the $NH_4V_4O_{10}$ after cycled in $Zn(OTf)_2$ (which is denoted as $NVO_{OTf\text{-}SO4}$). JCPDS # 31-0075 and # 41-1421 correspond to $NH_4V_4O_{10}$ and $Zn_{12}(OTf)_9(OH)_{15}\cdot nH_2O$[31], respectively.

To verify the above calculations and the proposed strategy, we carried out systematic experimental investigations. A typical cathode material for AZIBs, $NH_4V_4O_{10}$, was selected to study the properties of the CEI. The nanosheet morphology of the material, the chemical state of the V element, and the pure phase of $NH_4V_4O_{10}$ are presented in Figure 2a-c. After cycling the $NH_4V_4O_{10}$ cathodes (denoted as NVO) in $Zn(OTf)_2$ and $ZnSO_4$ electrolytes (denoted as $NVO_{Zn(OTf)2}$ and NVO_{ZnSO4}, respectively), the formation of ZnOTf-LDH and $ZnSO_4$-LDH can be observed (Figure S2). Moreover, after cycling in a small amount of $Zn(OTf)_2$ (for subsequent cycling in the $ZnSO_4$ electrolyte, denoted as $NVO_{OTf\text{-}SO4}$), the in-situ formation of the ZnOTf-LDH can be observed (Figure 2c), which results in a larger contact angle of $NVO_{OTf\text{-}SO4}$ than NVO_{ZnSO4} (Figure S3), demonstrating the hydrophobicity of the fluorinated interphase. After being sonicated in the deionized water, the ZnOTf-LDH was still observed on the NVO electrode, indicating the robust integration between the ZnOTf-LDH and NVO (Figure S4).

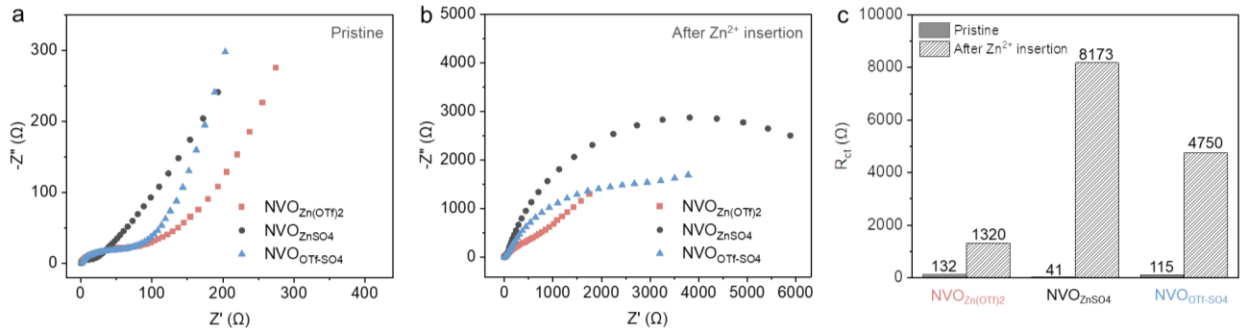

Figure 3. Staircase potential electrochemical impedance spectroscopy (SPEIS) investigations of the three samples of NVO in $ZnSO_4$ (NVO_{ZnSO4}), $NVO_{OTf-SO4}$, and NVO in $Zn(OTf)_2$ ($NVO_{Zn(OTf)2}$). (a) Nyquist plots at their pristine state. (b) Nyquist plots at their discharged state (first cycle). (c) Charge transfer resistance (R_{ct}) of the samples at pristine and after Zn^{2+} insertion states during the first discharge.

In order to get insights into the electrochemical mechanisms of $NVO_{Zn(OTf)2}$, NVO_{ZnSO4}, and $NVO_{OTf-SO4}$, impedance measurements, and GITT tests were performed. Firstly, through SPEIS investigations (Figure 3a,b), we obtain the evolution of interfacial charge transfer resistance (R_{ct}) for the three samples under in-situ and real-time conditions. After Zn^{2+} insertion, the order of R_{ct} presents $NVO_{ZnSO4} > NVO_{OTf-SO4} > NVO_{Zn(OTf)2}$ (Figure 3c).

To further understand the interfacial charge transfer process, impedance measurements were carried out at temperatures between 30-70 °C (Figures 4a-c). Through the fitting towards the plot of $\ln(R_{ct}^{-1})$ versus 1000/T (where T represents the Kelvin temperature), a precise determination of the activation energy (E_a) governing the interfacial charge transfer process was obtained. This insightful analysis was facilitated by applying the Arrhenius equation: $1/R_{ct} = A\exp(-E_a/RT)$. The results (Figure 4d) demonstrate that the E_a of $NVO_{OTf-SO4}$ (15.5 kJ mol^{-1}) is close to that of $NVO_{Zn(OTf)2}$ (14.2 kJ mol^{-1}) and smaller than that of NVO_{ZnSO4} (21.9 kJ mol^{-1}). The role of ZnOTf-LDH could thus be appreciated, as it not only helps to desolvate the Zn^{2+} but also allows them to go across the interface smoothly.

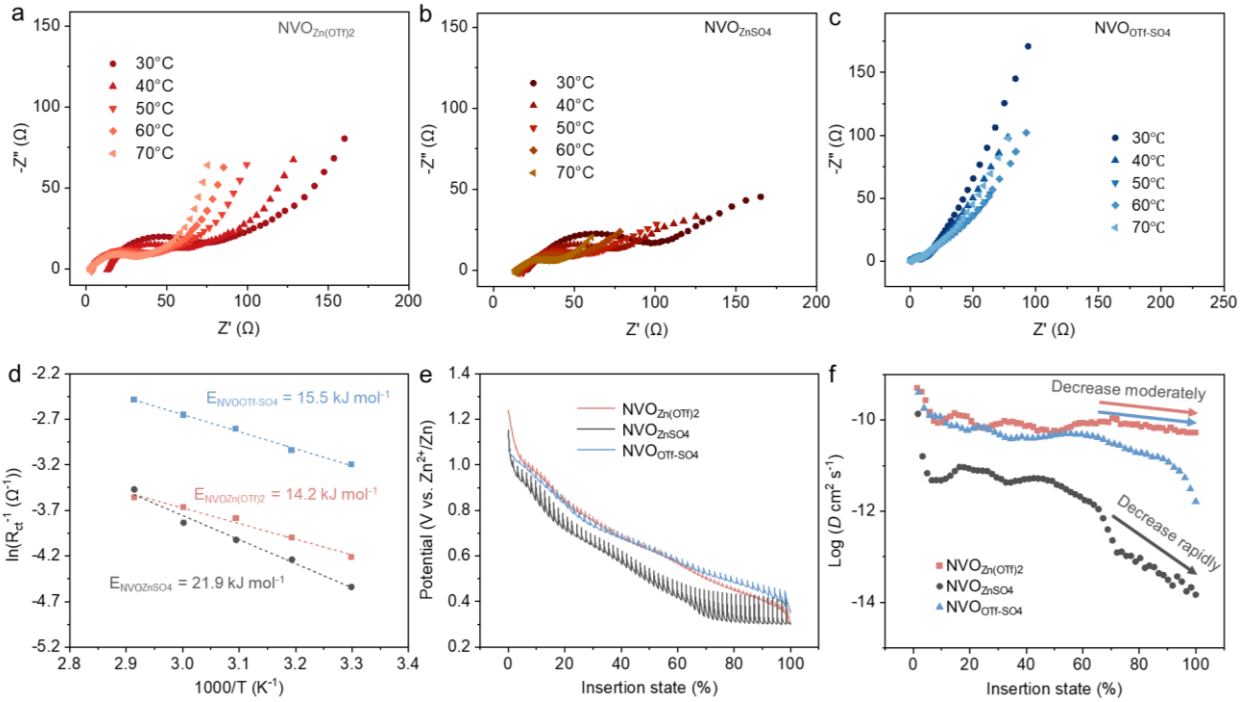

Figure 4. Impedance and diffusion behavior of the three samples including NVO_{ZnSO4}, $NVO_{OTf\text{-}SO4}$, and $NVO_{Zn(OTf)2}$. (a-c) Nyquist plots at different temperatures of (a) $NVO_{Zn(OTf)2}$, (b) NVO_{ZnSO4}, and (c) $NVO_{OTf\text{-}SO4}$. (d) Arrhenius plots of inverse R_{ct} (R_{ct}^{-1}) values at different temperatures. (e, f) Discharge GITT curves and corresponding Zn^{2+} diffusion coefficients versus discharge depth.

The GITT results provide further insights into ion migration within the NVO bulk (Figure 4c, d). The solid-state diffusion coefficient (*D*) values of $NVO_{OTf\text{-}SO4}$ and $NVO_{Zn(OTf)2}$ which are about 10^{-10} cm^2 s^{-1}, were found to be one order of magnitude higher than NVO_{ZnSO4} (~10^{-11} cm^2 s^{-1}). Remarkably, the *D* values of NVO_{ZnSO4} exhibit a rapid decrease at the discharge state of 66.6% (corresponding to a potential where Zn^{2+} intercalation occurs[32]), whereas the other two samples show a moderately decreasing trend. This phenomenon can be attributed to the solvation states of the intercalated ions. Specifically, considering that the radius of Zn^{2+} is 74 pm and $Zn(H_2O)_6^{2+}$ is 220 pm, the ZnOTf-LDH CEI contributes to desolvate hydrated ions and makes the intercalated ions more like bare Zn^{2+} (close to 74 pm). In comparison, the water-absorbing $ZnSO_4$-LDH CEI

promotes ion intercalation in a hydrated manner (close to 220 pm). As a result, the *D* value in NVO_{ZnSO4}. experiences a rapid decrease.

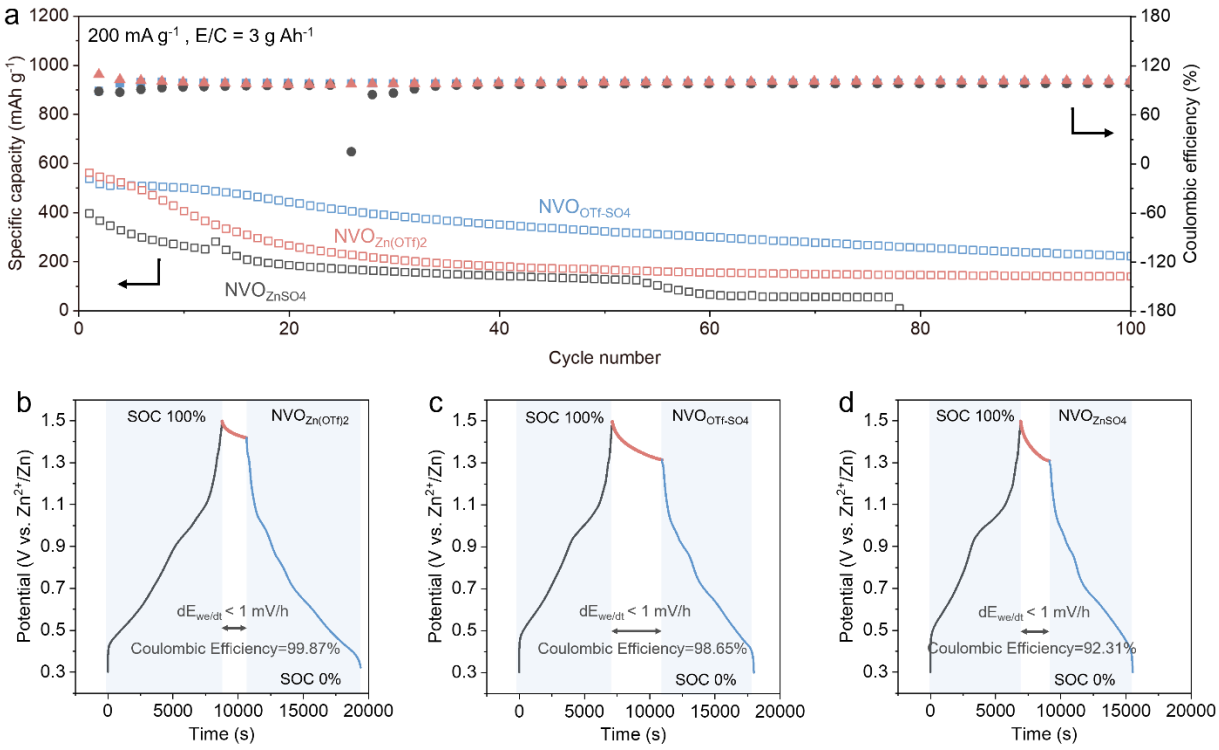

Figure 5. (a) Galvanostatic cycling performance and corresponding Coulombic efficiency of $NVO_{Zn(OTf)2}$, $NVO_{OTf\text{-}SO4}$, and NVO_{ZnSO4} at a current density of 200 mA g^{-1}, under a lean electrolyte condition (E/C = 3 g Ah^{-1}). Cells with (b) $NVO_{Zn(OTf)2}$, (c) $NVO_{OTf\text{-}SO4}$, (d) NVO_{ZnSO4} cathodes were firstly fully charged to 1.5 V at 200 mA g^{-1}, and then the cells were rested until dE/dt ≤ 1.0 mV/h, followed by full discharging to 0.3 V.

Further, we carried out charge/discharge cycling tests. As seen in Figure S5, the reaction mechanisms of the above three samples were basically consistent. Then, cycling performance was evaluated at a low current density of 200 mA g^{-1} (Figure 5a), with a specific focus on a lean electrolyte condition where the ratio of electrolyte amount to cathode capacity (E/C ratio) is 3 g Ah^{-1}.[33] Since the formation of LDHs in AZIBs consumes electrolytes, this lean electrolyte

condition reflects the more realistic performance of the battery. Due to the water-anchoring and Zn^{2+}-blocking effects of $ZnSO_4$-LDH, the $NVO_{OTf\text{-}SO4}$ shows faster capacity fading compared with the other two samples. Interestingly, $NVO_{OTf\text{-}SO4}$ exhibits a more stable cycling performance than $NVO_{Zn(OTf)2}$, which may be related to the fact that the Zn anode exhibits higher reversibility in the $ZnSO_4$ electrolyte than in the $Zn(OTf)_2$ electrolyte, resulting in a mitigated capacity fading at the anode side[34]. Moreover, the inhibited side reactions by the ZnOTf-LDH also make for excellent anti-self-discharge behavior of the Zn-NVO battery[35]. As shown in Figure 5b-d, after adequate rest, the $NVO_{Zn(OTf)2}$ and $NVO_{OTf\text{-}SO4}$ hold 99.87% and 98.65% of their original capacities, which are much better than that of NVO_{ZnSO4} (92.31% retention). This again indicates that the Zn-OTf is capable of suppressing the generation of by-products from water-related side reactions.

In summary, by targeting the two most commonly used electrolytes for AZIBs, namely $ZnSO_4$ and $Zn(OTf)_2$, we have revealed that the by-product of $ZnSO_4$-LDH in $ZnSO_4$ electrolytes blocks the diffusion channel for Zn^{2+} and severely anchors water leading to pronounced side reactions and high irreversibility. In contrast, ZnOTf-LDH enables the smooth passage of Zn^{2+} and promotes the desolvation of hydrated Zn^{2+}. Benefiting from this, the in-situ constructed CEI of ZnOTF-LDH exhibited good cycling stability at a low current density, ile utilizing a cost-effective and environmentally friendly $ZnSO_4$ electrolyte. This work provides insight into the role of LDH derived from different electrolytes in battery degradation and offers a truly effective and possibly universal approach to improving the cycling stability of AZIBs.

ASSOCIATED CONTENT

Supporting Information. The Supporting Information includes Experimental details and additional characterization data.

AUTHOR INFORMATION

Corresponding Author

*E-mail: jiantao_word@126.com (Jiantao Li), yazhou@mpip-mainz.mpg.de (Yazhou Zhou), junzoelu@zju.edu.cn (Ju Lu)

‡These authors contributed equally to this work.

Notes

The authors declare no competing financial interest.

ACKNOWLEDGMENT

We thank the financial support from the Max Planck Society, the National Natural Science Foundation of China (51702129 and 51972150), and the Postdoctoral Science Foundation (2018M630527 and 2019T120459).

REFERENCES

(1) Larcher, D.; Tarascon, J.-M. Towards greener and more sustainable batteries for electrical energy storage. *Nat. Chem.* **2015**, *7*, 19-29.

(2) Xu, C.; Li, B.; Du, H.; Kang, F. Energetic zinc ion chemistry: the rechargeable zinc ion battery. *Angew. Chem. Int. Ed.* **2012**, *51*, 933-935.

(3) Liu, Y.; Lu, X.; Lai, F.; Liu, T.; Shearing, P.-R.; Parkin, I.-P.; He, G.; Brett, D. Rechargeable aqueous Zn-based energy storage devices. *Joule* **2021**, *5*, 2845-2903.

(4) Nam, K.-W.; Kim, H.; Beldjoudi, Y.; Kwon, T.-W.; Kim, D.-J.; Stoddart, J.-F. Redox-active phenanthrenequinone triangles in aqueous rechargeable zinc batteries. *J. Am. Chem. Soc.* **2020**, *142*, 2541-2548.

(5) Yan, L.; Zhang, Y.; Ni, Z.; Zhang, Y.; Xu, J.; Kong, T.; Huang, J.; Li, W.; Ma, J.; Wang, Y. Chemically self-charging aqueous zinc-organic battery. *J. Am. Chem. Soc.* **2021**, *143*, 15369-15377.

(6) Zhao, K.; Fan, G.; Liu, J.; Liu, F.; Li, J.; Zhou, X.; Ni, Y.; Yu, M.; Zhang, Y.; Su, H.; Liu, Q.; Cheng, F. Boosting the kinetics and stability of Zn anodes in aqueous electrolytes with supramolecular cyclodextrin additives. *J. Am. Chem. Soc.* **2022**, *144*, 11129-11137.

(7) Service, R.-F. Zinc aims to beat lithium batteries at storing energy. *Science* **2021**, *372*, 890-891.

(8) Kundu, D.; Adams, B.; Duffort, V.; Vajargah, S.; Nazar, L. A high-capacity and long-life aqueous rechargeable zinc battery using a metal oxide intercalation cathode. *Nat. Energy* **2016**, *1*, 16119.

(9) Pan, H.; Shao, Y.; Yan, P.; Cheng, Y.; Han, K.; Nie, Z.; Wang, C.; Yang, J.; Li, X.; Bhattacharya, P.; Mueller, K.; Liu, J. Reversible aqueous zinc/manganese oxide energy storage from conversion reactions. *Nat. Energy* **2016**, *1*, 16039.

(10) Fang, G.; Zhou, J.; Pan, A.; Liang, S. Recent advances in aqueous zinc-ion batteries. *ACS Energy Lett.* **2018**, *3*, 2480-2501.

(11) Ming, F.; Zhu, Y.; Huang, G.; Emwas, A.; Liang, H.; Cui, Y.; Alshareef, H. Co-solvent electrolyte engineering for stable anode-free zinc metal batteries. *J. Am. Chem. Soc.* **2022**, *144*, 7160-7170.

(12) Liu, H.; Wang, J.; You, Z.; Wei, C.; Kang, F.; Wei, B. Rechargeable aqueous zinc-ion batteries: Mechanism, design strategies and future perspectives. *Mater. Today* **2021**, *42*, 73-98.

(13) Li, C.; Jin, S.; Archer, L.; Nazar, L. Toward practical aqueous zinc-ion batteries for electrochemical energy storage. *Joule* **2022**, *6*, 1733-1738.

(14) Zhang, N.; Cheng, F.; Liu, Y.; Zhao, Q.; Lei, L.; Chen, C.; Liu, X.; Chen, J. Cation-Deficient Spinel $ZnMn_2O_4$ Cathode in $Zn(CF_3SO_3)_2$ Electrolyte for Rechargeable Aqueous Zn-Ion Battery. *J. Am. Chem. Soc.* **2016**, *138*, 12894-12901.

(15) Kidanu, W.; Hur, J.; Choi, H. Kim, M.; Kim, I. High capacity and inexpensive multivalent cathode materials for aqueous rechargeable Zn-ion battery fabricated via in situ electrochemical oxidation of VO_2 nanorods. *J. Power Sources* **2022**, *523*, 231060.

(16) Blanc, L.; Kundu, D.; Nazar, L. Scientific challenges for the implementation of Zn-ion batteries. *Joule* **2020**, *4*, 771-799.

(17) Verma, V.; Kumar, S.; Manalastas, W.; Srinivasan, M. Undesired reactions in aqueous rechargeable zinc ion batteries. *ACS Energy Lett.* **2021**, *6*, 1773-1785.

(18) Wang, L.; Huang, K.; Chen, J.; Zheng, J. Ultralong cycle stability of aqueous zinc-ion batteries with zinc vanadium oxide cathodes. *Sci. Adv.* **2019**, *5*, eaax4279.

(19) Dai, Y.; Liao, X.; Yu, R.; Li, J.; Li, J.; Tan, S.; He, P.; An, Q.; Wei, Q.; Chen, L.; Hong, X.; Zhao, K.; Ren, Y.; Wu, J.; Zhao, Y.; Mai, L. Quicker and more Zn^{2+} storage predominantly from the interface. *Adv. Mater.* **2021**, *33*, e2100359.

(20) Wan, F.; Zhang, L.; Dai, X.; Wang, X.; Niu, Z.; Chen, J. Aqueous rechargeable zinc/sodium vanadate batteries with enhanced performance from simultaneous insertion of dual carriers. *Nat. Commun.* **2018**, *9*, 1656.

(21) Bin, D.; Huo, W.; Yuan, Y.; Huang, J.; Liu, Y.; Zhang, Y.; Dong, F.; Wang, Y.; Xia, Y. Organic-inorganic-induced polymer intercalation into layered composites for aqueous zinc-ion battery. *Chem* **2020**, *6*, 968-984.

(22) Huang, J.; Wang, Z.; Hou, M.; Dong, X.; Liu, Y.; Wang, Y.; Xia, Y. Polyaniline-intercalated manganese dioxide nanolayers as a high-performance cathode material for an aqueous zinc-ion battery. *Nat. Commun.* **2018**, *9*, 2906.

(23) Li, Z.; Ganapathy, S.; Xu, Y.; Zhou, Z.; Sarilar, M.; Wagemaker, M. Mechanistic Insight into the Electrochemical Performance of Zn/VO2 Batteries with an Aqueous ZnSO4 Electrolyte. *Adv. Energy Mater.* **2019**, *9*, 1900237.

(24) Oberholzer, P.; Tervoort, E.; Bouzid, A.; Pasquarello, A.; Kundu, D. Oxide versus nonoxide cathode materials for aqueous Zn batteries: an insight into the charge storage mechanism and consequences thereof. *ACS Appl. Mater. Interfaces* **2019**, *11*, 674-682.

(25) Jia, X.; Liu, C.; Neale, Z.; Yang, J.; Cao, G. Active materials for aqueous zinc ion batteries: synthesis, crystal structure, morphology, and electrochemistry. *Chem. Rev.* **2020**, *120*, 7795-7866.

(26) Wang, X.; Zhang, Z.; Xi, B.; Chen, W.; Jia, Y.; Feng, J.; Xiong, S. Advances and perspectives of cathode storage chemistry in aqueous zinc-ion batteries. *ACS Nano* **2021**, *15*, 9244-9272.

(27) Li, C.; Kingsbury, R.; Zhou, L.; Shyamsunder, A.; Persson, K.; Nazar, L. Tuning the solvation structure in aqueous zinc batteries to maximize Zn-ion intercalation and optimize dendrite-free zinc plating. *ACS Energy Lett.* **2022**, *7*, 533-540.

(28) Wang, F.; Blanc, L.; Li, Q.; Faraone, A.; Ji, X.; Chen-Mayer, H.; Paul, R.; Dura, J.; Hu, E.; Xu, K.; Nazar, L.; Wang, C. Quantifying and suppressing proton intercalation to enable high-voltage Zn-ion batteries. *Adv. Energy Mater.* **2021**, *11*, 2102016.

(29) Zhang, N.; Chen, X.; Yu, M.; Niu, Z.; Cheng, F.; Chen, J. Materials chemistry for rechargeable zinc-ion batteries. *Chem. Soc. Rev.* **2020**, *49*, 4203-4219.

(30) Sun, W.; Wang, F.; Zhang, B.; Zhang, M.; Kupers, V.; Ji, X.; Theile, C.; Bieker, P.; Xu K.; Wang, C.; Winter, M. A rechargeable zinc-air battery based on zinc peroxide chemistry. *Science* **2021**, *371*, 46-51.

(31) Li, Q.; Liu, Y.; Ma, K.; Yang, G.; Wang, C. In situ Ag nanoparticles reinforced pseudo-Zn-air reaction boosting $Ag_2V_4O_{11}$ as high-performance cathode material for aqueous zinc-ion batteries. *Small Methods* **2019**, *3*, 1900637.

(32) Zuo, S.; Liu, J.; He, W.; Osman, S.; Liu, Z.; Xu, X.; Shen, J.; Jiang, W.; Liu, J.; Zeng, Z.; Zhu, M. Direct detection and visualization of the H^+ reaction process in a VO_2 cathode for aqueous zinc-ion batteries. *J. Phys. Chem. Lett.* **2021**, *12*, 7076-7084.

(33) Niu, C.; Pan, H.; Xu, W.; Xiao, J.; Zhang, J.; Luo, L.; Wang, C.; Mei, D.; Meng, J.; Wang, X.; Liu, Z.; Mai, L.; Liu, J. Self-smoothing anode for achieving high-energy lithium metal batteries under realistic conditions. *Nat. Nanotechnol.* **2019**, *14*, 594-601.

(34) Zhou, J.; Shan, L.; Wu, Z.; Guo, X.; Fang, G.; Liang, S. Investigation of V_2O_5 as a low-cost rechargeable aqueous zinc ion battery cathode. *Chem. Commun.* **2018**, *54*, 4457-4460.

(35) Sun, P.; Ma, L.; Zhou, W.; Qiu, M.; Wang, Z.; Chao, D.; Mai, W. Simultaneous regulation on solvation shell and electrode interface for dendrite-free Zn ion batteries achieved by a low-cost glucose additive. *Angew. Chem. Int. Ed.* **2021**, *60*, 18247-18255.